ELECTRONICALLY STEERED MULTI-BEAM ANTENNA ARRAY PERFORMANCE AND BEAM TRACKING IN MOBILITY

Bahadir Canpolat
SatixFy UK Ltd., 279 Farnborough Road, Farnborough, UK GU14 7LS,
Tel: +44-1252933555,
bahadir.canpolat@satixfy.com
Divaydeep Sikri
SatixFy UK Ltd., 279 Farnborough Road, Farnborough, UK GU14 7LS,
Tel: +44-1252933553,
sikri.divaydeep@satixfy.com
Cetin Altan
SatixFy UK Ltd., 279 Farnborough Road, Farnborough, UK GU14 7LS,
Tel: +44-1252933577,
cetin.altan@satixfy.com

Abstract

In this paper, real-time performance measurement results of a digital electronically steered multi-beam antenna (ESMA) system are presented for static and mobility conditions using actual signals from active satellites. The system is designed to support Ka band, Ku band and L-band. It consists of 256 element antenna panel, RFIC units and multi-beam capable digital beamformers supporting up-to ~1 Gbps data speed. Modem interface is provided via a high-speed digital SERDES interface. Beam-forming is achieved with digital phase shifters; however, in order to improve the performance, true time delay is also supported for wide-band signals. The system is designed to be scale-able to support more elements (512, 1024, … etc.).

For the performance measurements, transmitter and receiver radiation patterns are obtained in an anechoic chamber and also in Satixfy's antenna micro test range set-up (AMTR). Moreover, transmitter tests and receiver SNR measurements are carried out using actual satellite signals. Efficient calibration algorithms are designed to make sure that the actual radiation patterns are close to theoretical which involves gain, phase and delay calibration. The system supports both linear and circular polarization and simultaneous multi-polarization operation is also possible.

In order to support all constellations including MEO and LEO and to maintain good Rx signal quality in mobility, tracking algorithms are needed to continuously adjust the beam steering angles to track the satellites and/or to counteract the changes in the antenna orientation due to terminal movement in applications such as land mobile, maritime and aero. Mobility tests have been performed which included driving tests to assess the tracking performance.

1   Introduction

In a previous study [1], we discussed the structure and architecture of a fully digital TTD (True Time Delay) wideband beamforming array in which the performance and limits of such an antenna array was addressed taking into account several factors and impact of impairments (phase noise, random phase and gain errors), grating lobes, and intra/inter satellite suppression. In this paper, we present a digital electronically steered multi-beam antenna array (ESMA) developed by Satixfy Ltd and its performance in mobility conditions against live active satellites.

To our knowledge, ESMA is the first fully digital multi-beam electronically steered antenna array implementation in the world, which has successfully been demonstrated to be able to track the signals from active satellites with an equivalent Tx and Rx performance as the comparable dish antennas offer in terms of EIRP and Rx SNR. Unlike the tracking dish antennas, ESMA does not have any moving part, and is

considerably smaller and lighter than them. Its fast-tracking functions, TTD feature and capability of supporting many beams simultaneously make it superior to its analog electronic beam steering antenna array counterparts in terms of performance and range of applications.

The ESMA comprises of 256 Tx/Rx patch antennas connected to RFIC and digital beam-former chips (see figures). This allows the user to obtain the benefit of array gain due to an 16x16 square array with one board, and 16x32 array with the use of two boards. The architecture is scalable to support up-to thousands of antenna elements depending on the requirements. There are two HW versions of the antenna array, one supporting Ku band and the other supporting Ka band. Prototype antennas are already available (Figure 1) that support Ku band, and development and design of Ka-band antenna array and RFIC is ongoing.
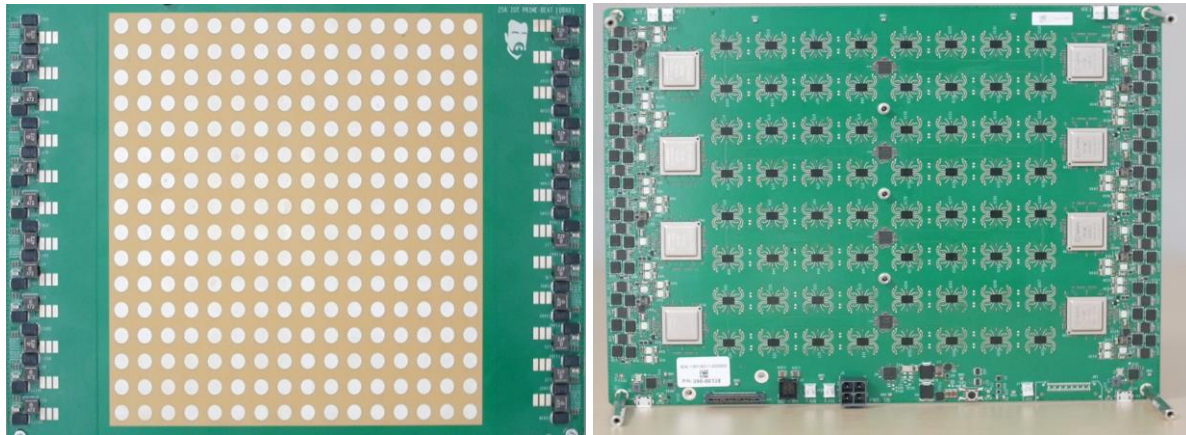

Figure 1 Front and rear-view of 16x16 ESMA digital beam-forming array

The role of antenna arrays in digital communications are increasing due to introduction of large capacity wireless access systems demanding high spectral efficiencies which are required by 5G and IOT terminal connectivity. Multi-Input Multi-Output (MIMO) antenna arrays has now become an integral part of the standards for cellular and wireless local area networks in current and future generations ([4]). These active antenna arrays will play an equally important role in next generation high throughput-satellite (HTS) communications. Also, with introduction of large LEO and MEO constellations, there is a growing need for antennas at ground terminals tracking multiple satellites. The parabolic dish antennas have been de-facto satcom earth antenna thus far because of mostly fixed pointing for GSO applications and in (quasi) static conditions. These antennas have their advantages from cost and power consumption but also are extremely inflexible and have lower efficiencies. On the other hand, electronically steerable antennas are active scanning antennas that provide many benefits such as self-installation capabilities, multi-satellite communication and satellite tracking. Payloads can be made more flexible and enable techniques such as multibeam, beam hopping and flexible beam shaping. Electronic control removes the need for moving mechanical parts, which are slow and more prone to malfunctions. High-speed tracking, which is required for LEO/MEO satellite communications and/or in mobility conditions (land mobile, maritime or aero) can also be accomplished more efficiently via electronic beam steering.

The paper is organized as follows: Section 2 discusses the high-level design and mathematical description of the digital multibeam TTD antenna arrays. Main features of the ESMA digital antenna array are also presented. Section 3 is allocated to calibration procedure and its performance. Section 4 is devoted to the results of Rx and Tx performance tests using actual signals from live satellites when the antenna is in static condition and steered to the satellites. Finally, in section 5, we present the tracking algorithms and performance under mobility conditions.

2   Multi-beam Digital Beamformer

2.1   Mathematical Model of Digital Beam Former

Figure 2 below depicts the array geometry for 1-D and 2-D square arrays where array centre is at the origin in both cases.
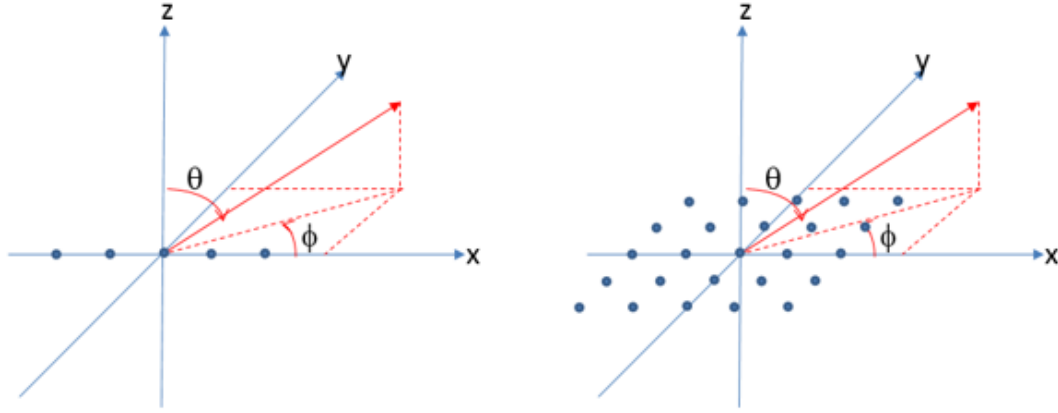

Figure 2- Antenna array geometry (1D and 2D)

Let the signal to be transmitted denoted by x(t). After digital beam-forming, the signal at the output at the antenna element (m,n) of the square antenna array is given as

$$s_{mn}(t) = \sqrt{P_{mn}} \ \underbrace{x(t + \tau_{mn})}_{\text{Delay adjustment}} \ \underbrace{exp(j\varphi_{mn})}_{\text{Phase Adjustment}}$$

$$\varphi_{mn} : 2\pi f_c(t + \tau_{mn})$$
$$\tau_{mn} = \frac{1}{c}(x_{mn} \cos \phi_0 + y_{mn} \sin \phi_0) \sin \theta_0 \qquad \text{[2.1]}$$

where, P_{mn} is the transmitted power for element indexed by (m, n),

f_c is the carrier frequency,

ϕ_0, θ_0 are the azimuth and polar steering angles

xx_{mn}, y_{mn} are the x and y distances of the element (m, n) to the array centre.

Note that the distance between two elements is assumed to be $\lambda/2$ in order to avoid grating lobes and minimize mutual correlation.

The radiated signal at any point (Φ,θ) in far-field, where Φ denotes the azimuth angle and θ denotes the polar angle with respect to the array center, can then be expressed as follows:

$$y(t; \theta, \phi) = G(\theta, \phi) \sum_{n=0}^{N-1} \sum_{m=0}^{N-1} s_{mn}\big(t - \mu_{mn}(\theta, \phi)\big)$$

$$= G(\theta, \phi) \sum_{n=0}^{N-1} \sum_{m=0}^{N-1} \sqrt{P_{mn}} x\big(t + \tau_{mn} - \mu_{mn}(\theta, \phi)\big) exp\left(j2\pi f_c\big(t + \tau_{mn} - \mu_{mn}(\theta, \phi)\big)\right)$$

$$\mu_{mn}(\theta, \phi) = \frac{1}{c}(x_{mn} \cos \phi + y_{mn} \sin \phi) \sin \theta$$

$G(\theta, \phi)$: Patch antenna gain   [2.2]

From [2.1], it can be observed that beam-forming requires phase offsets as well as delay offsets in the input signal. If the baseband signal is narrowband or if the number of elements is small, then the following approximation holds

$$x(t + N\tau) \sim x(t), \text{ for } N\tau \ll T_s = \frac{1}{BW}$$

[2.3]

where N denotes the number of antennas in one dimension. If the above approximation holds, delay offset in the signal for each element can be ignored, but if it does not hold, the delay in baseband signal cannot be ignored and contributes to frequency selective fading or inter-symbol interference if not compensated. Therefore, depending on the signal bandwidth, one can have two operation modes, where the only phase corrections are applied in the first mode (PA: Phased Array), and in the other, both phase and delay differences between antenna elements are compensated (TTD: True Time Delay).

$$y(t) = \sum_{m=0}^{N-1} \sum_{n=0}^{N-1} y_{mn}(t)\exp(-j\varphi_{mn}) \text{ (PA mode)}$$

[2.4]

$$y(t) = \sum_{m=0}^{N-1} \sum_{n=0}^{N-1} y_{mn}(t - \mu_{mn})\exp(-j\varphi_{mn}) \text{ (TTD mode)}$$

[2.5]

The main advantage of PA mode is its simplicity which leads to less power consumption relative to the TTD mode. PA mode is the only practically possible mode of operation for the analog beam-formers. As long as the signal bandwidth is small and/or the number of antennas is small, PA mode may be the preferred mode of operation. However, when the signal bandwidth and/or number of antennas increase, ignoring the delay compensation may result in beam squint issues that cause antenna defocussing whereby antenna gain becomes frequency dependent. On the other hand, the True Time Delay, which corrects for both Delay and Phase provides completely beam-squint free performance as shown in the previous study [1]. Therefore, for wide-band applications, performance of the TTD digital beam-former is superior than that of a digital or analog phased-array beam-former, which can only do phase offsets and ignore delay offsets.

Figure below shows a mathematical description of the True Time Delay Beamformer with both Delay and Phase compensation.

In the RX side, the signal received at each element is demodulated from RF to Baseband. For digital beamformer, the signal will then be digitized with processing shifting to discrete signal domain via A/D. This will be then followed by delay correction in the digital domain which corrects the delay to within certain residual delay error limit that allows [2.3] to hold for the wideband signal. Delay adjustment is followed by Phase correction (not necessarily in the same order) and the signals are then combined to produce beamformed signal. Within digital domain, the delay correction can be implemented with good precision and at very low cost.

The RFIC designed and used in the antenna array supports both linear (V and H) and circular (LHCP and RHCP) polarisation. Prototypes supporting Ku band (GHz in Rx, GHz in Tx) are already available, but Ka band version of the RFIC is still in the design phase. Therefore, the test results presented in subsequent sections belong mostly to Ku-band.
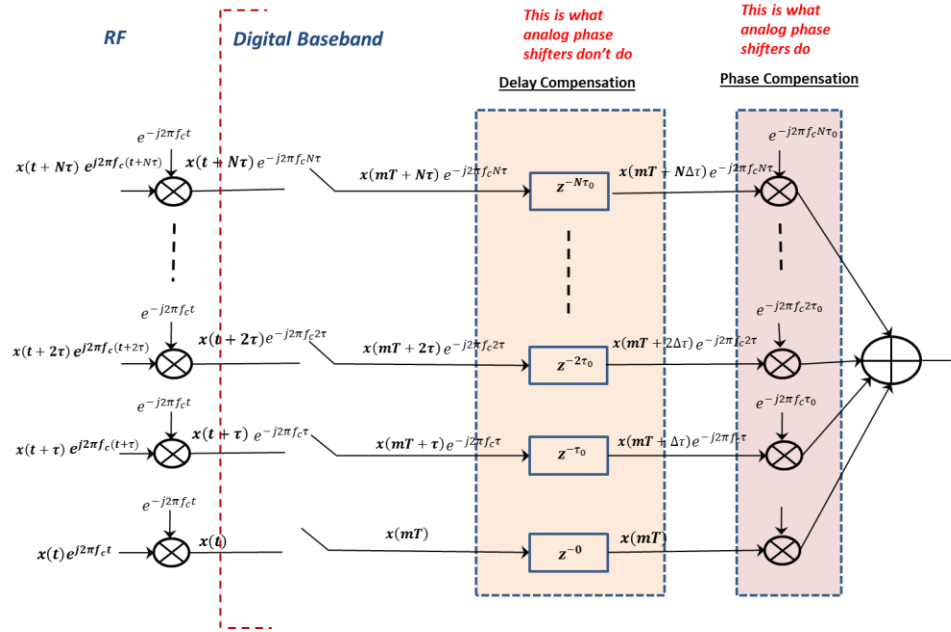
Figure 3 Mathematical Description of True Time Delay Digital Beamformer

Table below summarizes the main characteristics of Satixfy's digital beamforming antenna array, ESMA.

Number of elements	256 (16x16)
	Scale-able to 512 (2 panels) or more (e.g. 1024, 2048 etc)
Beam width (at bore-sight)	~6°for 16x16
Side-lobes	13 dBc (without tapering)
	<30 dBc (with Taylor window tapering)
Operation frequencies (Analog RFIC)	Ku: 10.75-12.7 GHz (Rx), 14-14.5 GHz (Tx)
	Ka: 22.55-23.15 GHz (Tx), 25.5-27 GHz (Rx)
Number of beams	Up-to 32
Typical EIRP (dBW), Tx	256 elements: 26 dBW, 512 elements: 32 dBW
Typical G/T, dB, Rx	256 elements: 1-2 dB/K
Signal Bandwidth	Up-to 880 MHz (≤ 2 beams)
	Up-to 440 MHz (≤ 4 beams)
	Up-to 220 MHz (≤ 8 beams)
	Up-to 110 MHz (≤ 16 beams)
	Up-to 55 MHz (≤ 32 beams)
Modem interface	Analog L-band interface per beam through a special adapter unit, or high-speed digital SERDES interface

Table 1 Properties of ESMA digital multi-beam antenna array

2.2 Multi-beam Operation

One of the main advantages of digital beam-forming is the ability to support multiple beams simultaneously, where the number of beams may be as high as 32 (or even more) in practical applications. Such a feat is generally not possible for analog beam-formers which requires complete duplication of the Tx and Rx circuits for each beam added, which practically limits their operation to support only a single beam, or at most two beams.

Multi-beam operation enables make-before-break by tracking two satellites simultaneously. By increasing the number of beams, the tracking performance and/or UL or DL throughput can be improved significantly. Also, it is possible to simultaneously connect to two or more multiple satellites using the same antenna, if their operation frequencies lie in the same band (Ku or Ka band), which offers significant operational (performance, power consumption and cost) advantages.

From the digital beam-forming perspective which employs both delay and phase adjustment, the concept of multi-beam is straightforward. In the transmitter, multiple signals are separately phase shifted and delayed for each antenna element and then they are simply summed up in digital domain. The available transmitter power is usually divided equally between the beams, which means individual beams have less power. The transmitted signal for each element for an M-beam signal can be expressed as follows:

$$y_i(t) = \frac{P_t}{M} \sum_{m=1}^{M} x_m(t - \tau_{mi}) e^{j\psi_{mi}}, 1 \leq i \leq N_{ant} \qquad [2.5]$$

In the receiver, the received signal is applied different phase and delay offsets for individual beams and signals from all antennas are combined separately for each received beam.

Figure below depicts a 4-beam radiation pattern (dBW) vs polar angle for a 64 element array.
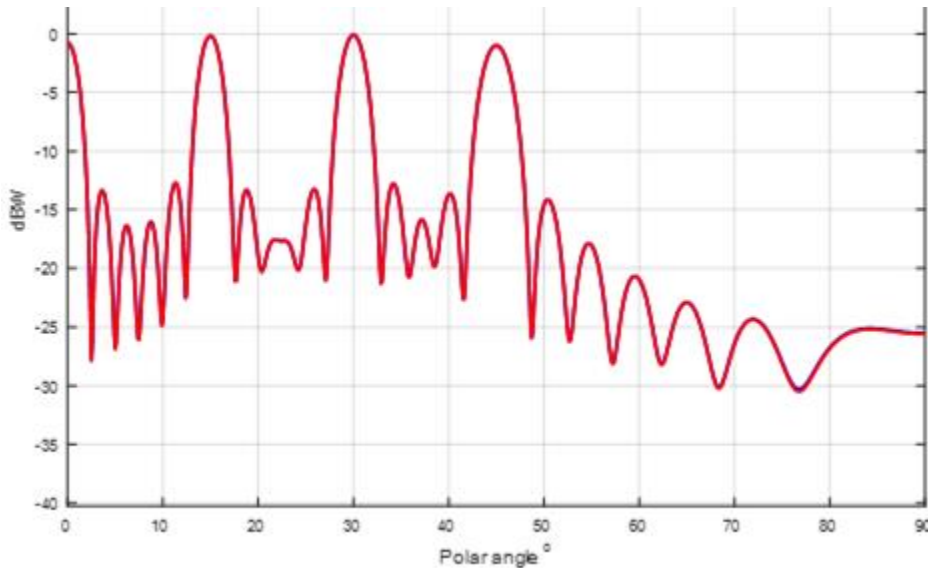

Figure 4 Multi-beam Tx Radiation pattern (64x1 array, 4-beams, no tapering)

3   Calibration of the Digital Beamformer

Calibration is one of the most important factors that must be taken into account in practical applications. The objective is to compensate for the inherent gain, delay and phase offsets between the elements that arise from the imperfection of the components. Such phase and delay offsets are naturally not part of beam-forming offsets and must therefore be compensated for otherwise significant beam pointing errors and off-axis transmission violations may occur.

As discussed in [1]**Error! Reference source not found.**, understanding the sources of phase and delay errors within a beamformer array is crucial for calibration and therefore successful synchronization of the system.

ANTENNA   RF   ADC   IF   INTRA-CHIP   INTER-CHIP

$r_n^1(t)$ → $Z^{-\tau_{ant}^n}$ → $r_n^2(t)$ → $r_n^3(t)$ → $Z^{-\tau_{RP}^n}$ → $r_n^4(t)$ → $Z^{-\tau_{ADC}}$ → $r_n^5(t)$ → $r_n^6(t)$ → $Z^{-\tau_{dig}^n}$ → $r_n^7(t)$ → $Z^{-\tau_{IC}^n}$ → $r_n^8(t)$

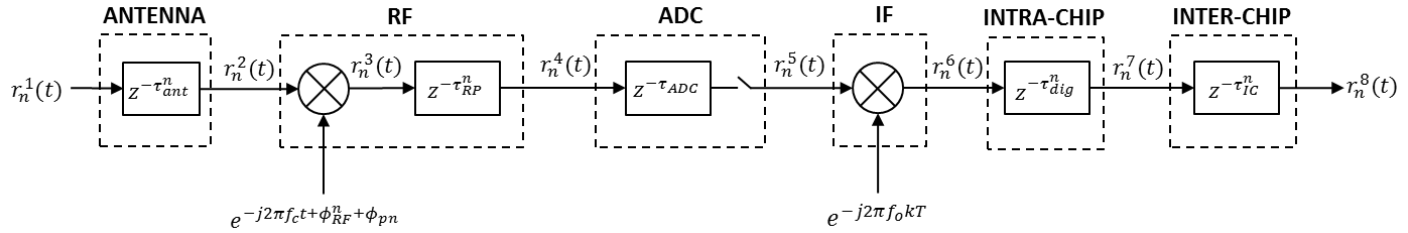$e^{-j2\pi f_c t + \phi_{RF}^n + \phi_{pn}}$

$e^{-j2\pi f_o kT}$

Figure 5 Internal Sources of Phase and Delay Errors at an antenna element [1]

Figure 5 depicts the various sources of delay and phase error within analogue and digital domains considered at a single chain of the beamforming array. A cumulative delay and phase error estimation within specification limits is expected to suffice for most practical system calibration purposes. Ideally, one-time factory calibration would suffice which may include different calibration data based on different temperature ranges and frequency bands. However, over-the-air (OTA), or run-time calibration may also be required in order to compensate for the significant deviations that are detected in the relative phase offsets between the elements during the operation. For the purpose of this study, we only considered static (offline) calibration, which requires the characterization of phase, delay and gain offsets between the elements. Characterizations are done for Tx and Rx separately, and for each different frequency band of operation and polarization, and for different temperature ranges. In the context of the tests presented in this paper, we considered 4 different temperature ranges for the calibration (extreme low, low, nominal room and extreme hot temperatures).

Relative phase and gain estimations are done using a signal generator and horn antenna (for transmitting the reference signal) for Rx, and a spectrum analyzer and a horn antenna (for receiving the signals transmitted by the array elements) for Tx. In each case, horn antenna gain, cable losses and free-space losses are precisely known. Relative gain and phase offsets are computed by measuring the relative offsets of the tested element against a selected element in the array that is designated as the reference. The basic idea is that making the gain and phase/delay of each element same as the reference compensates the relative offsets for all elements. Once those offsets are measured, they are stored in a calibration file that is later used in during the operation to compensate the phase/gain offsets between the elements.

The calibration procedure must be performed in an anechoic room which is large enough for far field measurements. If the array size is smaller (256 antennas or less in Ku or Ka band) and effects due to near-field measurements can be ignored, the smaller setups may be used like Satixfy's antenna micro test range (AMTR) that is shown in Figure 6

Figure 6 Antenna Micro Test Range (AMTR)

In Figure 7 below, radiation pattern of 256 element antenna array is shown that is obtained immediately after calibration of the transmitter in anechoic chamber without power cycle of the unit. As can be seen from the figure, the radiation pattern is in perfect agreement with the theoretical expectations. In Figure 8, radiation patterns are shown after power cycling the unit several times and loading/applying the previously calculated calibration data for 256 elements. As can be seen from the figure, calibration data remains valid after power cycling and the pattern remains in close agreement with the initial run in which fresh calibration data is applied. This means that, for most cases, the same calibration data can be used repeatedly without the need of run-time re-calibration (for the same frequency band and temperature range). Please note that switching to a different calibration table in run-time in case of significant temperature change or change in frequency is still regarded as part of the offline calibration process as it does not require run-time re-characterization of relative gain and phase offsets between antenna elements.
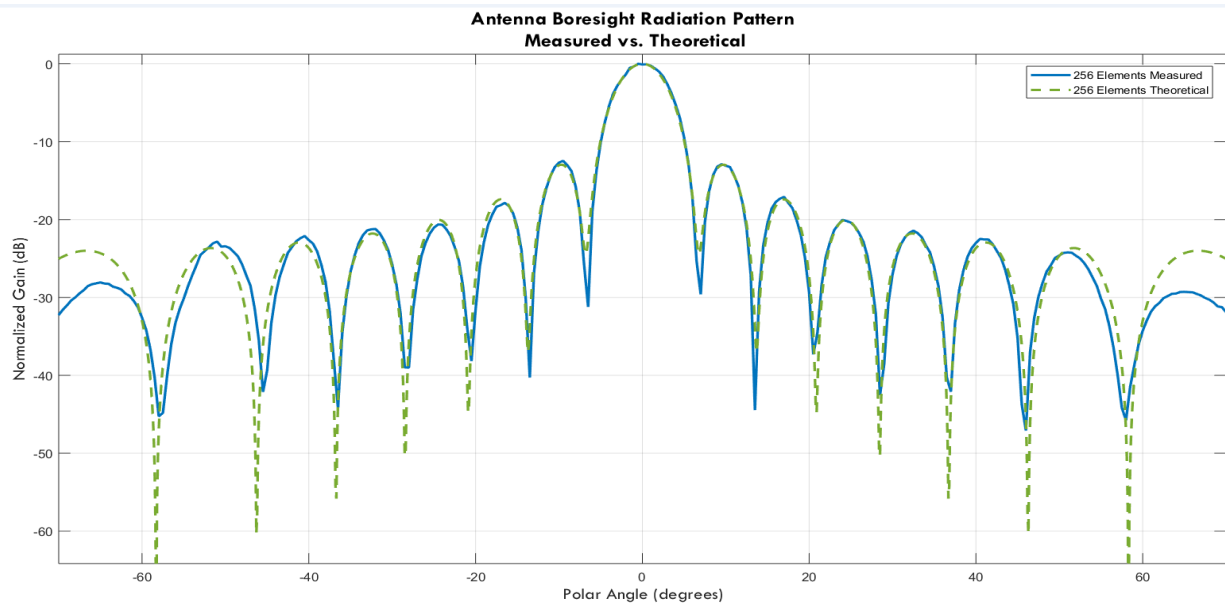

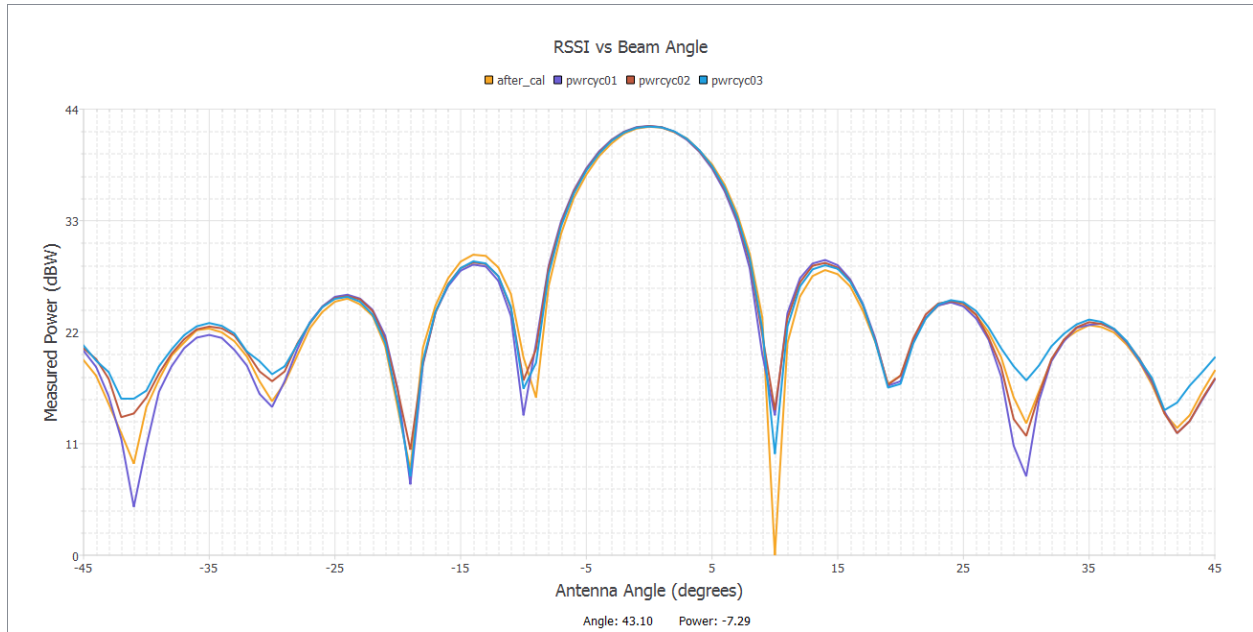Figure 7 Measured radiation pattern for 16x16 array

Figure 8 Radiation pattern measurements after power cycle with loaded calibration data

4   Static Tests against Active Satellites

Before attempting to track active live satellites in mobility conditions, the tests are first performed in static conditions, by manual application of the electronic beam steering in static conditions against non-moving (i.e. GEO) satellites. In the first round of tests, one 16x16 panel for Rx (256 antennas in total) and two 16x16 panels for Tx (512 antennas) are used. Two different satellites are used for this test, both operating in Ku-band. Static calibration data are obtained in the far-field anechoic chamber for each satellite frequency/polarisation, and for 4 different temperature ranges, for Rx and Tx separately.

Test setup is diagrammatically shown in the figures below for Rx and Tx tests. Note that the satellite is acting as bent-pipe in both cases and hence UL traffic is same as DL traffic for the return link.
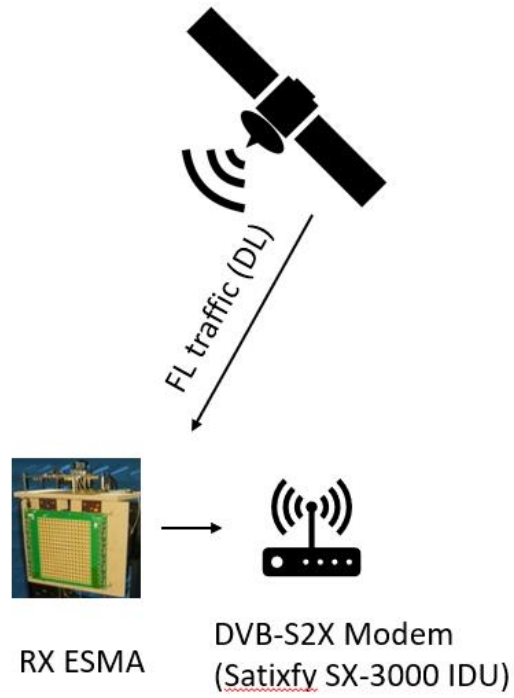
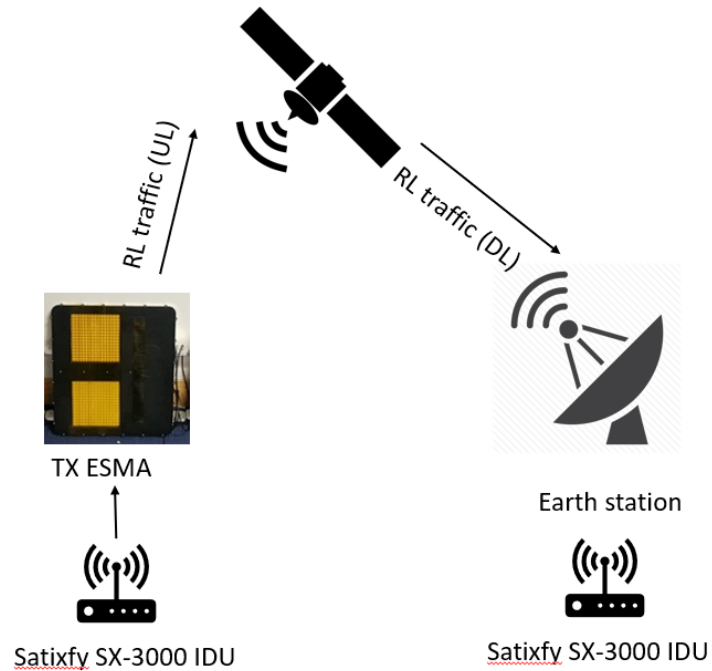Figure 9 Rx test set-up (static) on the forward-link downlink

Figure 10 Tx test set-up (static) on the return link.

TX tests	Satellite 1	Satellite 2
RL UL frequency	14.13025 GHz	14.1568 GHz
EIRP (ESMA)	32 dBW	32 dBW
Polarisation	Linear (V)	Linear (H)
Number of elements (ESMA)	512	512
Satellite elevation	25°	30°
Average SNR measured at the peer Rx modem	1 dB	5.5 dB
Signal BW	0.5 MHz (roll-off=0.2)	0.5 MHz (roll-off=0.2)
Signal (modulation, spread, Coding rate)	DVB-S2X VLSNR BPSK-SF2-1/5	DVB-S2X VLSNR BPSK-SF2-1/5 QPSK-SF1-13/45 16APSK-SF1-1/2 32 APSK-SF1-2/3
Measured data throughput	BPSK-SF2-1/5: 0.04 Mbps	BPSK-SF2-1/5: 0.044 Mbps QPSK-SF1-13/45: 0.28 Mbps 16APSK-SF1-1/2: 0.93 Mbps 32 APSK-SF1-2/3: 1.59 Mbps
RX tests	**Satellite 1**	**Satellite 2**
FL DL frequency	11.10625 GHz	11.739 GHz
Polarisation	Linear (H)	Linear (V)
Number of elements (ESMA)	256	256
Measured G/T, dB of ESMA (*)	1.5	2
Satellite elevation	25°	30°
Measured SNR at FL modem (typical, clear skies)	-5 dB	1 dB
Signal BW	0.5 MHz (roll-off=0.2)	27.5 MHz (roll-off=0.2)
Signal (modulation, spread. Coding rate)	DVB-S2X VLSNR BPSK-SF2-1/5	DVB-S2X VLSNR BPSK-SF2-1/5
Measured data throughput	0.04 Mbps	2.2 Mbps
(*) G/T of the receiver antenna is computed as follows: G/T = SNR – EIRP + FSPL (Free Space Path Loss) – K (Boltzmann) + B (Bandwidth) FSPL is assumed to be 205.6 dB. K=228.6 dBW B = 10*log10(BW_Hz)		

Table 2 Results of static tests against two GEO satellites

Table above summarizes the test parameters and test results. Antennas are kept in a flat, fixed position and required beam steering to the target satellites are done via electronic steering. SNR and throughput results have also been confirmed to agree with those of reference dish featuring similar EIRP and G/T as ESMA, which shows that the digital beam-former is operating as expected.

Further static tests are under-way, in which 512 antennas will be used also for Rx instead of 256 elements and basic over-the-air run-time re-calibration/correction will be utilised both for Tx and Rx in addition to the static (offline) calibration. End-to-end throughput tests will be performed, too, in which Tx and Rx antennas will both be ESMA, communicating through a bent-pipe satellite.

5   Satellite Tracking in Mobility

In mobility conditions, the heading of the antenna against the satellite constantly varies therefore dynamic update of the beam angles are necessary to maintain the quality of the communication link with the satellite even if it is a GEO satellite. For LEO/MEO satellites, tracking of the satellite, and hence dynamic beam angles update is required even for static cases due to relative movement of the satellite with respect to the antenna user plane.

In this section, we will first discuss the satellite co-ordinate systems which is key to the operation of the tracking function. We will then discuss ephemeris-based tracking for LEO/MEO satellites. Finally, we will address open-loop and closed-loop beam tracking in mobility cases. Mobility test results (car tests) for open-loop tracking are also presented in sub section 5.3.

5.1   Co-ordinate Systems

There are two types of cartesian (xyz) inertial coordinate systems:

- Space-fixed or celestial
- Earth-fixed or terrestrial

The earth's rotation axis, which is connecting to the geo-center to the pole serves as the z-axis in both cases. The x-axis for the space-fixed system points towards the vernal equinox and is, thus, the intersection line between the equatorial and the ecliptic plane. The x-axis of the earth-fixed system is defined by the intersection line of the equatorial plane with the plane represented by the Greenwich meridian. The angle Θ_0 between the two systems is called Greenwich sidereal time.

In both cases, the third axis, i.e. y-axis, is orthogonal to both the x-axis and the z-axis and completes a right-handed coordinate frame ([5]) as shown in Figure 11. Terrestrial cartesian coordinate systems are also known as Earth-Centric Earth-Fixed (ECEF) coordinate systems.
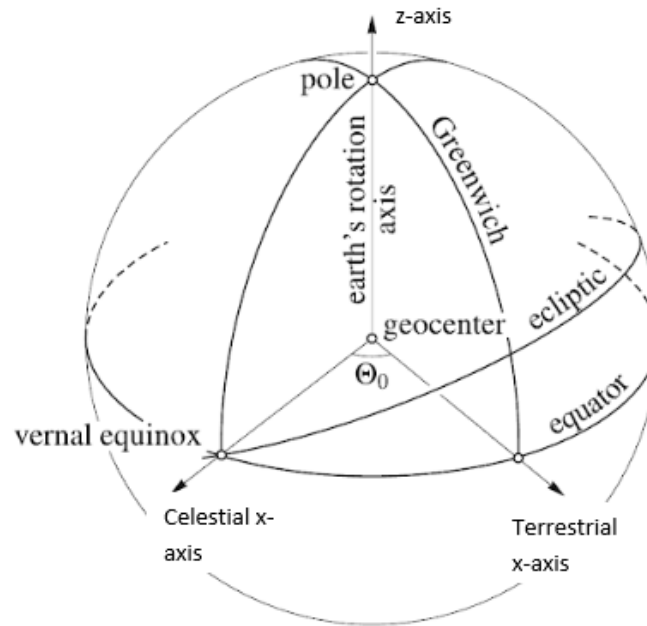

Figure 11 Space (celestial) and earth-fixed (terrestrial) coordinate systems

Once the coordinates of a point are determined in ECEF coordinate system, position of that point in ellipsoidal coordinates (known as latitude, longitude and altitude) can be determined as follows (Figure 12):

- **Geodetic Latitude (ϕ):** angle measured in the meridian plane through the point P between the equatorial plane of the ellipsoid and the line perpendicular to the surface of the ellipsoid at P
- **Geodetic Longitude (λ):** angle measured in the equatorial plane between the reference meridian and the meridian plane through P (positive east from the zero meridian)
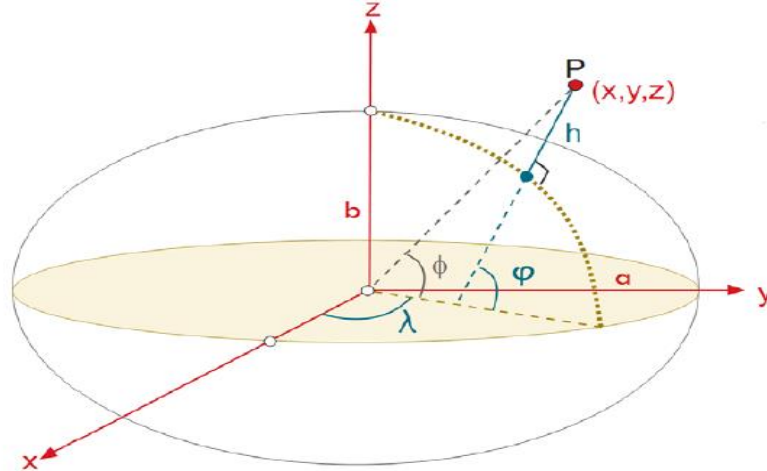- **Geodetic height(h):** measured along the normal to the ellipsoid through P.

Figure 12 Ellipsoidal terrestrial coordinate system

Closed and open-form expressions for cartesian to ellipsoidal coordinate conversion (and vice versa) can be found in numerous references, for example see [6].

5.2 Ephemeris based tracking of LEO/MEO satellites

Ephemeris-based tracking of a satellite which is in relative motion to the user antenna (even in static user conditions) attempts to do the followings:

- Determine the ephemeris (or almanac) parameters for the target satellite for orbit prediction.
- Determine the user antenna position in elliptical coordinates via a GNSS receiver (GPS, Galileo etc.)
- From the ephemeris data, derive the satellite position (in ECEF coordinates) using the algorithm described in this section
- Finally, determine the position of the satellite with the respect to user antenna coordinates in terms of user (elliptical) coordinates as azimuth and elevation and update beam steering accordingly.

In mobility cases, in which both the satellite and the antenna is moving relative to antenna's inertial reference frame, ephemeris-based tracking will be used in conjunction with the sensor-based tracking algorithm of section 5.3. Ephemeris based satellite coordinate estimation is also be used to determine the initial location of the satellite that is being tracked.

Ephemeris data that provides (sub-) meter level orbit information. Each satellite periodically transmits the ephemeris data for itself. Almanac data that provides coarse orbit information with a typical accuracy at the 1 km level to support the acquisition process. Each satellite transmits the orbit parameters of all satellites in the constellation along with auxiliary health and status information. The precise timing information is also sent along with the ephemeris or almanac data.

The full ephemeris data typically consists of 16 parameters (see, for example, [7]), also see Figure 13:

- 6 Keplerian parameters (e, A, i_0, Ω_0, ω, M_0), which are eccentricity, semi-major axis length, inclination angle, right ascension of the ascending node, argument of peri-apsis and mean anomaly.

- 6 harmonic coefficients (C_{uc}, C_{us}, C_{rc}, C_{rs}, C_{ic}, C_{is}) for corrections to argument of latitude, orbit radius and inclination angle
- 1 orbit inclination rate parameter ($\dot{i}$), which is the rate of change of inclination angle
- 1 RAAN rate parameter ($\dot{\Omega}$), which is the rate of change of the RAAN
- 1 mean motion correction parameter (Δn)
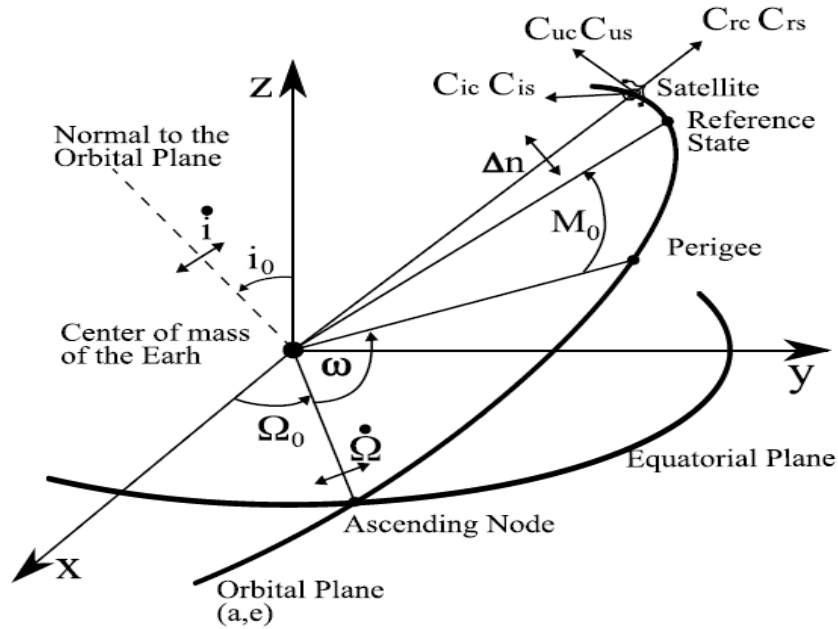- 1 reference time parameter for the ephemeris data set (t_{oe})

Figure 13 Orbit Parameters (Ephemeris)

Almanac parameters typically only contains only the 6 Keplerian parameters, RAAN rate parameter and mean motion correction parameter, together with the reference time information of the almanac data itself. Once ephemeris or almanac parameters are known, then the user can compute ECEF coordinates of the SV's <u>antenna phase center</u> position at any time t using the equations shown in table below (for reduced parameter case).

Computation	Description
$$n_0 = \sqrt{\frac{\mu}{A^3}}$$	Computed mean motion (rad/s), $\mu = GM_{earth}$ is the geocentric gravitational constant = 3.986004418x10^{14} m^3/s^2
$t_k = t - t_{0,a}$	Time from almanac reference epoch
$n = n_0 + \Delta n$	Corrected mean motion
$M = M_0 + nt_k$	Mean anomaly
$M = E - e\,sin(E)$	Kepler's equation for eccentric anomaly, which is solved by iteration

$v = tan^{-1}\left(\dfrac{\sqrt{1-e^2}/(1-e\cos E)}{(\cos E - e)/(1-e\cos E)}\right)$	True anomaly.
$\Phi = v + \omega$	Argument of latitude
$x^{'} = A(1-e\cos E)\cos\Phi$ $y^{'} = A(1-e\cos E)\sin\Phi$	Position in orbital plane
$x^{'} = \Omega_0 - \left(\dot{\Omega} - \omega_E\right)t_k - \omega_E t_{0,a}$	Corrected longitude of the ascending node. ω_E is the mean angular velocity of the Earth, which is 7.2921151467x10^{-5} rad/s
$x = x^{'}\cos(\Omega_0) - y^{'}\cos(i_0)\sin(\Omega_0)$ $y = x^{'}\sin(\Omega_0) + y^{'}\cos(i_0)\cos(\Omega_0)$ $z = y^{'}\sin(i_0)$	ECEF coordinates of the satellite antenna phase center position at time t

Table 3 Algorithm for estimating satellite ECEF coordinates from the reduced ephemeris data

Once the satellite position and user position in cartesian ECEF coordinates are known, satellite position with respect to user frame needs to be determined in terms of azimuth and elevation beam angles as shown in Figure 15 of the next section. These are then used in the beam angle updates to adjust the Tx or Rx beam angles to point to the current position of the satellite that is being tracked.

5.3 Open-Loop Tracking with INS

In order the electronically steered antenna terminal to be able to track its target (GEO, LEO or MEO satellite) while it is on the move, the system should know its orientation all the time. This is achieved by using inertial sensor data and incorporating an appropriate attitude estimation algorithm.

Open-loop tracking refers to the tracking algorithm which is based on the instantaneous position estimates derived from INS unit which uses multiple sensors. As opposed to closed-loop tracking, which is briefly discussed in the next chapter, it does not need to use receiver feed-back thanks to the availability of high accuracy orientation and position data, but this requirement also increases the overall cost of the unit.

In most cases, an inertial measurement unit (IMU) is used to provide the needed inertial data. Such a device consists of tri-axis gyroscope, accelerometer and possibly magnetometer. It measures accelerations and rotation rates, and earth's magnetic field, in order to estimate the body's attitude.

The raw data provided by the IMU is usually not reliable unless it is filtered. Therefore, all existing attitude estimation algorithms fuse the accelerometer, magnetometer and integrated gyroscope data. This is accomplished by passing the accelerometer data through a low pass, and the gyro data through a high pass filter, and then adding the outputs. This way, on the short term, the data from the gyroscope is used, because it is very precise and not susceptible to external forces, and on the long term, the data from the accelerometer (and magnetometer) is used, as it does not drift.

For attitude determination, commercial GNSS aided inertial navigation system (INS) units have been used, which employ an extended Kalman filter based sensor fusion of gyroscope, accelerometer and magnetometer data.

Orientation of a rigid body can be achieved by composing three elemental rotations, i.e. rotations about the axes of a coordinate system. The values of these three rotations are called Euler angles in honor of mathematician Leonhard Euler. These three angles are also known as Yaw, Pitch and Roll.
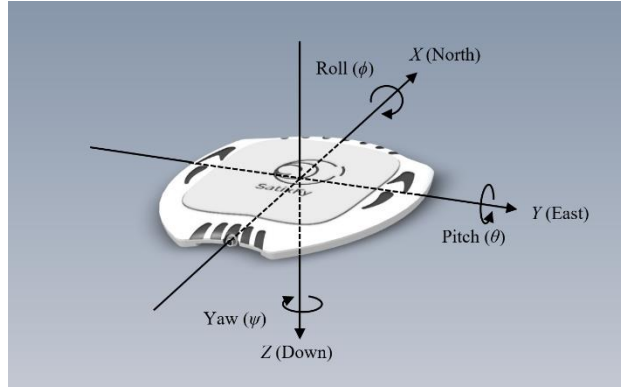
Figure 14 Orientation of a rigid body in 3D-space: Roll, yaw and pitch angles

Multiple coordinate frames are used to describe the orientation: the inertial frame and the body frame. The inertial frame axes are Earth-fixed, and the body frame axes are aligned with the antenna and the sensors that are used for the tracking. A common aeronautical frame is used where the x-axis points north, the y-axis points east, and the z-axis points up or down. It is called East-North-Up (ENU) or alternatively North-East-Down (NED) reference frame.

The diagram below summarizes the open-loop tracking algorithm. It follows the following steps:

- Current satellite coordinates are determined either via a data-base for GEO satellites, or via ephemeris-based tracking algorithm of section 5.2 for LEO/MEO satellites
- Current antenna coordinates are found via GNSS (e.g. GPS)
- Using these information, user plane coordinates and polarization skew factor is computed in ECEF coordinates as shown in the diagram.
- Attitude data in the form of roll, yaw and pitch angles are obtained via INS
- Finally, beam angles (azimuth and elevation angles) and polarization skew are updated to track the change in the satellite position with respect to the current orientation of the body/antenna frame. If there is a fixed offset between the body (sensor) frame and antenna frame, that should be compensated in the co-ordinate calculations and the final result should be provided with respect to the antenna frame.

The required beam update rate is a function of the desired max beam pointing error (ε) and the angular velocity of the relative motion of the antenna plane with respect to the satellite (ω) as follows

$$f_{Hz} = \frac{2\omega}{\varepsilon}$$

[5.2]

The angular velocity depends on the mobility settings. For example, in VSAT mobility specs [8], average angular velocity in the land-mobile conditions is given as 29 °/sec. For example, for RX antenna, to support tracking in such cases without significant loss in the RX SNR (within 0.5 dB) for a beam-width of 6° (256 antennas), the beam pointing error should ideally remain less than ~1.8 °. Using [5.2], this means that the beam update rate should be ~30 Hz or more.
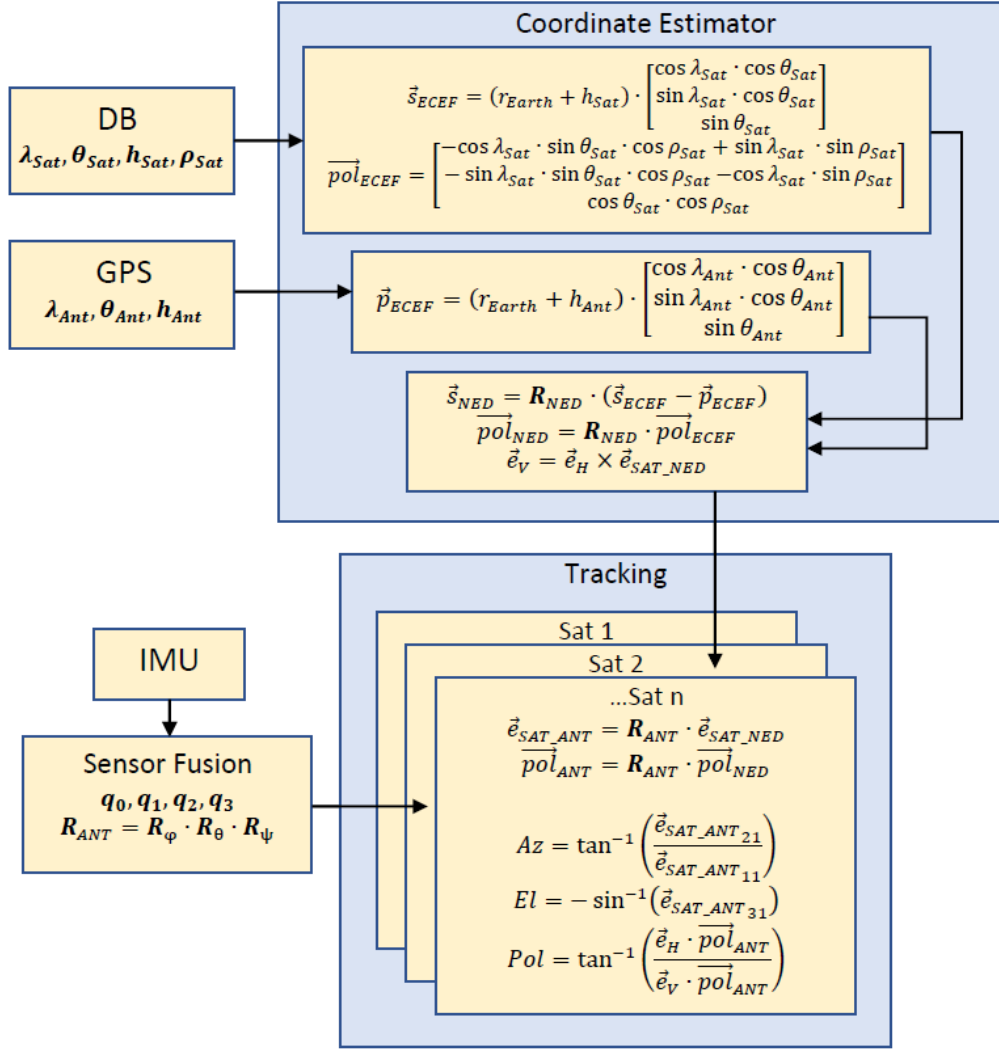
Figure 15 Open-loop tracking algorithm

5.4   Closed-loop Tracking

In closed-loop tracking, tracking beams that are set around the vicinity of the calculated main beam are used and by utilizing the receiver feed-back in closed-loop, the optimum beam position is determined adaptively and dynamically. The positioning sensors are still required in mobility conditions, but accuracy requirements are lower than those used in open-loop tracking since precision errors in the attitude and heading determination can be partially compensated by doing fine adjustments on the calculated beam angles by checking different hypotheses with the use of tracking beams through the receiver feed-back. In Rx tracking, the feed-back is obtained via the local modem and the digital beam-former (DBF) itself. In Tx case, a separate feed-back control link is required to receive the performance metric data (SNR and/or RSSI) from the peer Rx modem.

Figure 16 depicts closed-loop tracking flow diagram and the concept of tracking beams. The Rx feed-back will consist of RSSI readings from the digital beamformer and also post-demodulator SNR. For the different direction hypotheses for tracking beams, one main beam + 4 side beams are considered in the vicinity of the main beam position as shown in Figure 16.
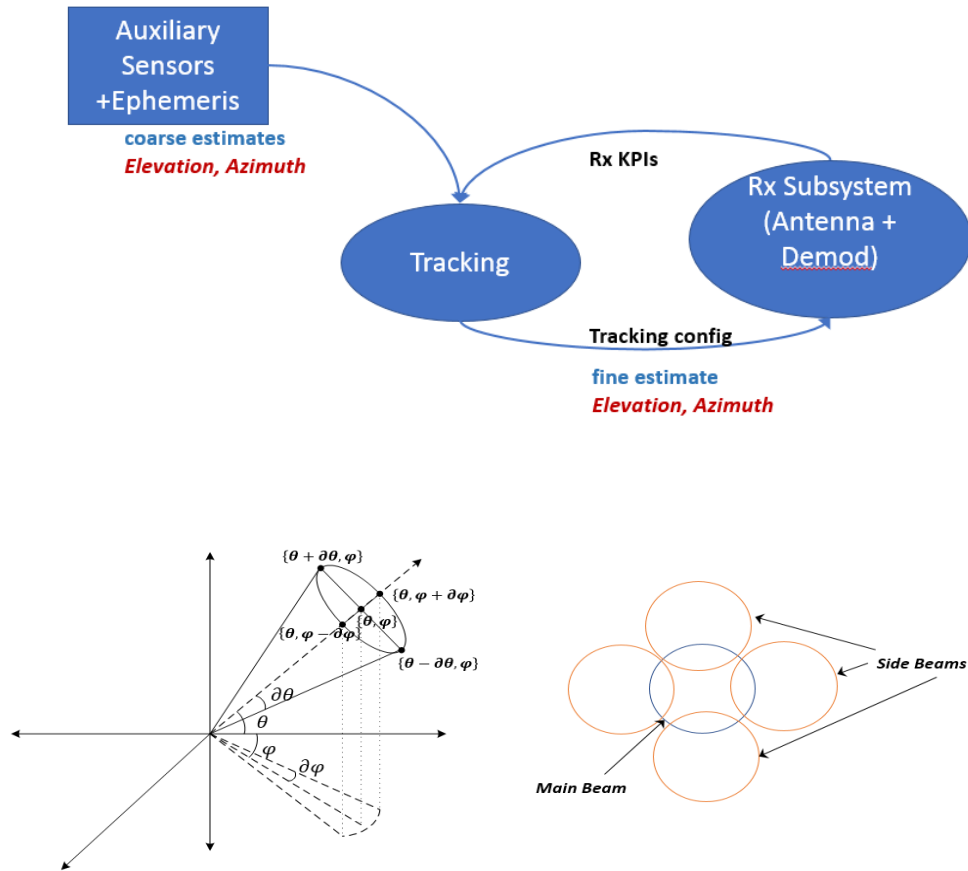
Figure 16 Closed-loop tracking with tracking beams

5.5   Drive Test Results

In order to verify the performance of the Tx and Rx antenna and tracking functions in mobility conditions, drive tests have been performed along the routes in mostly urban areas of Farnborough, UK. The antenna (256 elements Rx panel and 512 elements Tx panel) are placed flat in the back of a pick-up track using external car batteries for power supply.

Similar to the setting of the static tests shown in Figure 9 and Figure 10, the main performance metric is the post-demodulator SNR reported by the DVB-S2X modem (which is the Satixfy SX3000 IDU). For Rx tests, the modem is directly connected to the Rx antenna in the car. For Tx test, the modem is connected to the Rx dish in the Earth listening station that is tuned to the RL frequency of the Tx ESMA antenna transmission from the car. Satellite 1 (see section 4)has been used in the drive tests. DVBS2X VLSNR BPSK signal is used for the tests for 0.5 MHz transmission bandwidth. The following information is recorded continuously during the drive test:

- Rx demodulator SNR and lock status (in the car)
- Hub (Earth station) demodulator SNR and lock status
- Raw roll, yaw and pitch angles from the INS unit
- Calculated beam angles, azimuth and elevation (or polar angle)

Two antennas have been used to be able to maintain the line of sight with the satellite at any time, whereby one modem is connected to the antenna array on one side of the vehicle and the other modem is connected to the antenna on the other side of the vehicle. This makes it possible for most of the times at least one of the antennas can track the signal when the car is going in one direction or in opposite direction.

The figures below Rx SNR vs time and against the polar angle for the two modems. It has been observed from the results that for both Rx and Tx, tracking has been able to keep the link active with almost constant SNR as long as the antenna is within the field of view (FOV) of the satellite. The FOV limits typically depend on the by polar (90°-elevation) angle, which is typically between 0 to ~80° polar angles. Outside this range, it is not possible to establish the link with the satellite even in static case.

Open-loop tracking with INS has been used during the drive tests. The implementation/testing of the closed loop tracking is currently underway.
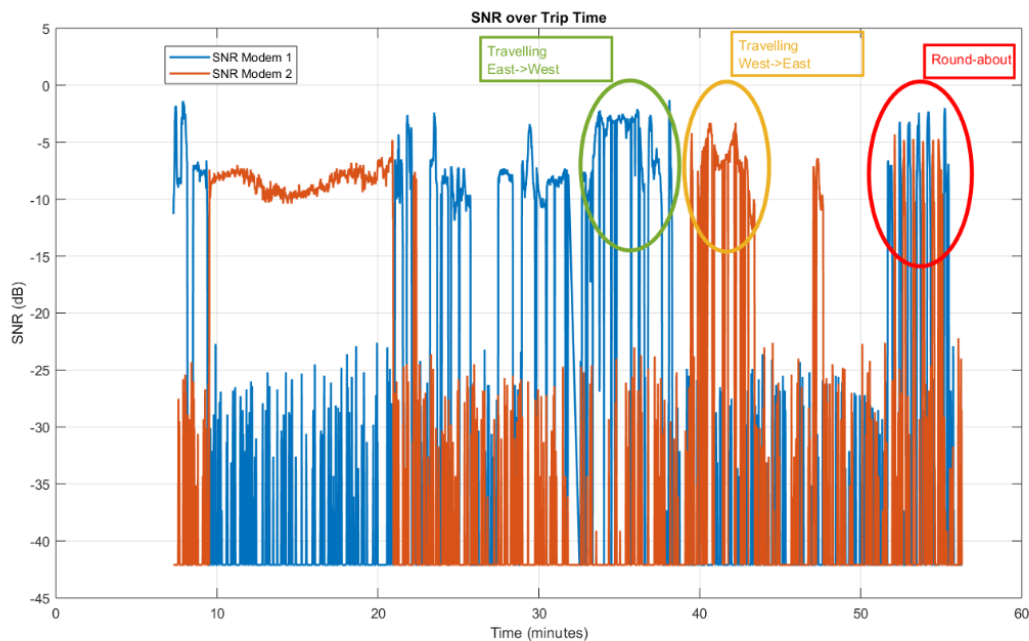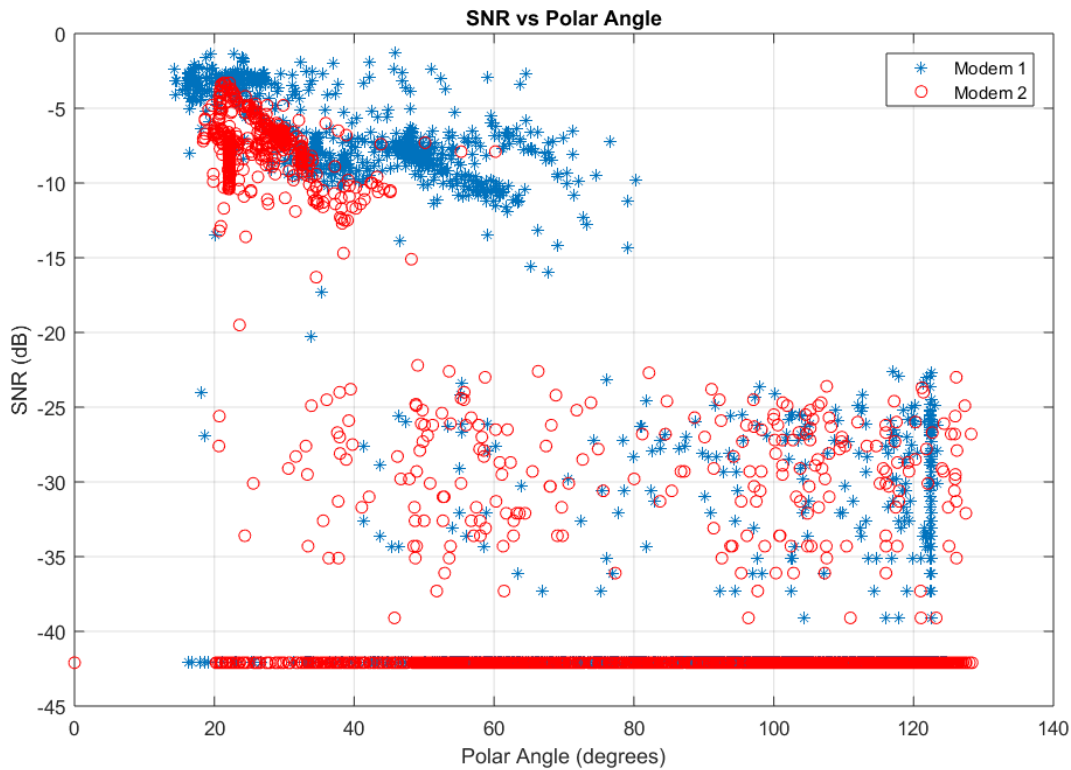

Figure 17 Drive test results: SNR vs time

Figure 18 Drive test results: SNR vs polar angle

References

[1] Sikri, D., Altan C., Canpolat B., "Digital Beam-former Array: Performance Analysis", *23rd Ka and Broadband Communications Conference*, Trieste, Italy, 2017

[2] Rainish, D., Freedman, A., "Low Cost Digital Beamforming Array Structure and Architecture", *22nd Ka and Broadband Communications Conference,* Cleveland, Ohio, October 2016.

[3] M. I. Skolnik, Introduction to Radar Systems, 3rd ed. New York, NY: McGraw-Hill, 2001.

[4] A.F. Molisch: *Wireless Communications*, John Wiley and Sons. 2nd ed. 2011

[5] Hoffmann-Wellenhof, Lichtenegger, Wasle, *GNSS Global Navigation Satellite Systems: GPS, GLONASS, Galileo, and More*, Springer, New York, 2008

[6] M.T.A. Alonso, "GNSS Reference Systems", *gAGE/UPC (Research group of astronomy and geomatics) Professional Training Program,* 2012

[7] "European GNSS (Galileo) Open Service Signal in Space Interface Control Document", *OS SIS ICD*, Issue 1.3, Dec 2016

[8] "Performance and Test Guidelines for Type Approval of 'Comms on the Move' Mobile Satellite Communication Terminals", Global VSAT Forum Specification GVF-105, Jan 2016